

Article

A Nonlinear Dynamic Model for Characterizing the Downhole Motions of the Sidetracking Tool in a Multilateral Well

Xiuxing Zhu ¹ , Weixia Zhou ¹, Yujian Lei ¹, Peng Jia ¹, Shifeng Xue ^{1,*}, Bo Zhou ^{1,*} and Yuanbo Xia ²

¹ College of Pipeline and Civil Engineering, China University of Petroleum (East China), Qingdao 266580, China

² CNPC Tianjin Bo-Xing Engineering Science & Technology Co., Ltd., Tianjin 300451, China

* Correspondence: sfeng@upc.edu.cn (S.X.); zhoubo@upc.edu.cn (B.Z.)

Abstract: It is of practical interest to investigate the mechanical behaviors of a sidetracking tool system and to describe the sidetracking tool's vibration mechanical response, as this can provide an important basis for evaluating and optimizing the tool structure and effectively controlling the profile of the sidetracking window. In this article, three nonlinear dynamic models with ten, six, and two degrees of freedom, respectively, are established using the Lagrange method to characterize the behavior of the sidetracking tool. It should be noted that in these models, the axial, lateral, and torsional vibration of the tool system are fully coupled. The process of the sidetracking tool mills in the casing-pipe wall is divided into three typical stages, i.e., the window mill, pilot mill, and watermelon mill grinding the casing, respectively. The dynamic response of the three stages is studied to more effectively analyze the influence of the sidetracking tool vibration deformation on the window width. The Runge–Kutta method, which is easy to implement, is applied to solve the supposed nonlinear dynamic model, and some useful findings are as follows. The effects of sidetracking tool vibrations at different stages on window widening size are illustrated quantitatively. The vibration trajectory pattern of the sidetracking tool is different from that of the conventional drilling tool due to the influence of the whipstock, which changes from the general whirling motion pattern to the X reciprocating pattern, and the vibration amplitude decreases. Due to the influence of the tool's lateral amplitude, the window profile is widened. The widened window size of the window mill and the pilot mill are 3.30 mm and 2.74 mm, respectively, and the extended window size of the watermelon mill is 0.07 mm, while the maximum window width formed by the sidetracking tool is 374.34 mm. This work proposes, for the first time, the coupled vibration model of the sidetracking tool system, which is helpful to better understand the nonlinear dynamic effects of the sidetracking tool, laying the foundation for the optimization of the sidetracking parameters.



Citation: Zhu, X.; Zhou, W.; Lei, Y.; Jia, P.; Xue, S.; Zhou, B.; Xia, Y. A Nonlinear Dynamic Model for Characterizing the Downhole Motions of the Sidetracking Tool in a Multilateral Well. *Energies* **2023**, *16*, 588. <https://doi.org/10.3390/en16020588>

Academic Editors: Mofazzal Hossain, Md Motiur Rahman and Hisham Khaled Ben Mahmud

Received: 24 November 2022

Revised: 28 December 2022

Accepted: 31 December 2022

Published: 4 January 2023



Copyright: © 2023 by the authors. Licensee MDPI, Basel, Switzerland. This article is an open access article distributed under the terms and conditions of the Creative Commons Attribution (CC BY) license (<https://creativecommons.org/licenses/by/4.0/>).

Keywords: window milling; sidetracking tool; nonlinear dynamics; vibration; window profile

1. Introduction

The casing window sidetracking technology is widely used in the recovery of residual oil in aged oil fields, especially in multilateral wells [1,2]. Its aim is to cut out a slanting and smooth window at the designated position on the casing wall of the original well hole by using sidetracking tools along the whipstock [3,4]. The huge expansion of sidetracking technology has facilitated the application of an increasing number of sidetracking systems, in which tool systems have had a significant impact on the success of sidetracking. A bottom-hole sidetracking tool system typically consists of a window mill, a flexible joint, and a watermelon mill. The tool diameter is generally smaller than the casing diameter, providing a gap for the tool to deform and move due to weight on bit and torque [5]. Thus, the motion of a sidetracking tool is a multi-coupled nonlinear motion that includes rotations around its geometric axis, roll, and rotational motion around the drilling axis,

etc. These complex motions increase the uncertainty of the tool motion and make it more difficult to predict the profile of the sidetracking window.

The vibration of the sidetracking tool system during drilling is an unavoidable phenomenon due to the combined effects of weight on bit, torque, and reaction forces on the casing wall. This phenomenon consists of three different types of vibrations, namely longitudinal, transverse, and torsional. The longitudinal vibration is the most harmful [6–8]. Tool vibrations can cause tool system failure, accelerate casing wear, and reduce device safety. It is worth noting that the most intense vibration occurs at the bottom of the well, so it is extremely essential to analyze the vibration characteristics of the bottom hole assembly [9].

Regarding the reduction of unnecessary losses caused by tool vibration during sidetracking, there are numerous previous articles in the literature that have addressed the stick-slip phenomenon in drill string vibration, and these studies have proposed methods for its control. S. H. Choi et al. [10] gave a consistent derivation of a set of governing differential equations and proposed a different method to correctly calculate the axial load effect of the Timoshenko beam. However, the coupling between the bending and torsional vibrations due to mass eccentricity is not considered in this work. H. Ahmadian et al. [11] adopted the Lagrange method to obtain the control equation of drill string motion considering the coupling of axial, lateral, and torsional vibrations and proposed a fully coupled model, calculated the contact force between the drill collar and borehole wall, and studied its behavior. K. Nandakumar et al. [12] established a fully coupled two degree of freedom model, which consisted of two coupled delay differential equations, assuming a state-dependent delay and viscous damping for both axial and torsional motions. They conducted a detailed linear stability analysis of the obtained mathematical model. This work provides a reference for subsequent research on drill string vibration. Luciano P.P. de Moraes et al. [13] studied the coupled vibration of a drill string considering the four degrees of freedom non-smooth model, with parametric studies of bit bounce, stick-slip, rotation, and combination effects. Dou Xie et al. [14] developed a dynamic model of the drill string in horizontal wells with six degrees of freedom, considering longitudinal, lateral, and torsional motions. State-dependent time delays were introduced during the cutting process to couple the axial and torsional motions of the bit. Mohammadzadeh Maziar et al. studied the fully coupled nonlinear vibrations drill string, which is a composite drill string consisting of orthogonal anisotropic layers, using the Lagrange method and finite element methods and investigated the analytical capability of the dynamic model [15]. Then, they also studied the ability of the composite drill string, with different configurations, to track and transmit the fully coupled nonlinear vibration [16]. All the above studies have led to advances in the study of vibrational properties of drill strings. However, if these theories are to be applied to the sidetracking aspect, further analysis is needed to continue to consider the effects of the whipstock and milling tools.

In addition, the drill string vibrations have been investigated for control and energy conversion. Wang Peng et al. [17] developed a unified mathematical model considering the two mechanisms of static and dynamic friction conversion and friction decomposition. The model was solved by the second-order finite difference method to obtain the variations of weight on bit, drilling speed, and positive displacement motor tool face under three different sliding drilling methods. Tian Jialin et al. established the multi degrees of freedom torsional vibration model and the nonlinear dynamic model of the drill string, which is a new torsional vibration tool. They studied the viscosity reduction mechanism combined with the actual working conditions in the drilling process [18]. Then, they established the drill string axial-torsional-lateral coupled vibration model. The coupled vibration sliding mode PI controller was designed to control and analyze the drill string system [19]. Ritto Thiago G. et al. [20] proposed an active vibration control method, which considered a simplified two-DOF drill string torsion model. Through experiments, Xu Yuqiang et al. [21] studied the characteristics of downhole bit load and drill string longitudinal vibration under different conditions. Significantly, they proposed an energy conversion efficiency analysis method converting the drill string vibration to spring po-

tential energy. Sassi Sadok et al. [22] conducted an experimental study on the suppression of drill string vibration using a new drill string design. More recently, AmirNoabahr Sadeghi et al. [23] subdivided the drill string into smaller torsional segments and modeled the whole system dynamically. Mathematically by modeling stick-slip vibrations using an extracted torsion model, three structures have been developed and proposed to reduce and actively control stick-slip vibrations, namely, speed control, bit-weight control, and increasing damping at the bottom of the drill string.

In the process of milling window, the behavior of the bottom hole assembly (BHA) affects the deformation and geometry of the milling tool, and then affects the movement of the BHA. Therefore, the mechanical analysis of BHA is also extremely crucial. Sarker Mejbahul et al. [24] presented a model to analyze the dynamics of a horizontal oil well bottom hole assembly. The model can predict how axial and torsional bit-rock reactions are propagated to the surface and the role that lateral vibrations near the bit play in exciting those vibrations, as well as the stressing components in the bottom-hole-assembly. Liu Yongsheng et al. [25] developed a nonlinear dynamic model with four degrees of freedom (DOF) to characterize the behavior of the drill string in a deviated well. This study provided a theoretical understanding of the drill string nonlinear motion in non-vertical wells. Wang Jin et al. [26] analyzed the dynamics model of a rotary steerable system (RSS) with a single stabilizer and flexible joint, and simplified the drill collar and joint to obtain a suitable BHA mechanical analysis model and a finite element analysis model. However, these studies do not take into account the interaction between the drill string and the casing. Thus, the results for the mechanical behavior of the BHA cannot be reflected in the window profile model.

The above research results mainly focus on the vibration of the drilling tool in the drilling process, while there are few studies on the vibration deformation of the sidetracking tools. Particularly, there are few reports on the model considering the influence of the sidetracking tool vibration on the window shape under the action of construction parameters such as weight on bit. Therefore, studying the force of the sidetracking tool in the drilling process and establishing the vibration models in different drilling stages is essential. The second section of this paper depicts the 2-DOF system considered in the analyses, as well as the control strategies employed. The third section presents the numerical results and, finally, the concluding remarks are presented in the last section.

2. Dynamic Model of Sidetracking Tool

As shown in Figure 1, the physical model of the sidetracking tool has three key parts: the watermelon mill, the pilot mill, and the window mill [27]. These three parts have different operating conditions, so their dynamic behavior will be discussed separately.

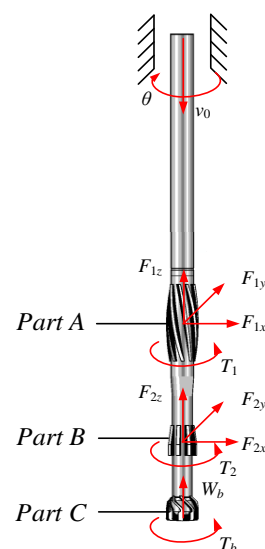


Figure 1. Physical model of the sidetracking tool.

2.1. Model Simplification of the Sidetracking Tool

For the ideal sidetracking tool considered, the assumptions are as follows: (1) The drill hole is straight, and its diameter is equal to the drill bit diameter. (2) The damping effect of the drilling fluid is neglected [28]. Based on these assumptions, a lumped mass model is proposed, which consists of three parts, as shown in Figure 1. In this system, the inertial characteristics of the watermelon mill, pilot mill, and window mill are represented by Part A, B, and C, respectively. These three parts are connected with each other through the elastic section string.

According to the physical model of the sidetracking tool, the dynamics of Parts A and B are described by four degrees of freedom, i.e., one longitudinal, one torsional, and two transverse, respectively. The dynamic characteristics of Part C are described by only two degrees of freedom, longitudinal and torsional, because its lateral motion is limited by the whipstock. This system is driven from the top with constant axial velocity v_0 and constant angular velocity $\dot{\varphi}_t = \theta$. In Figure 2, the subscripts 1 and 2 of each physical quantity represent Part A and Part B, respectively. The subscripts x and y represent the lateral direction, respectively, and z represents the axial direction. W_b represents the weight on bit. T_b represents torque, and T_i ($i = 1\sim 2$) represents friction torque. F represents the contact force.

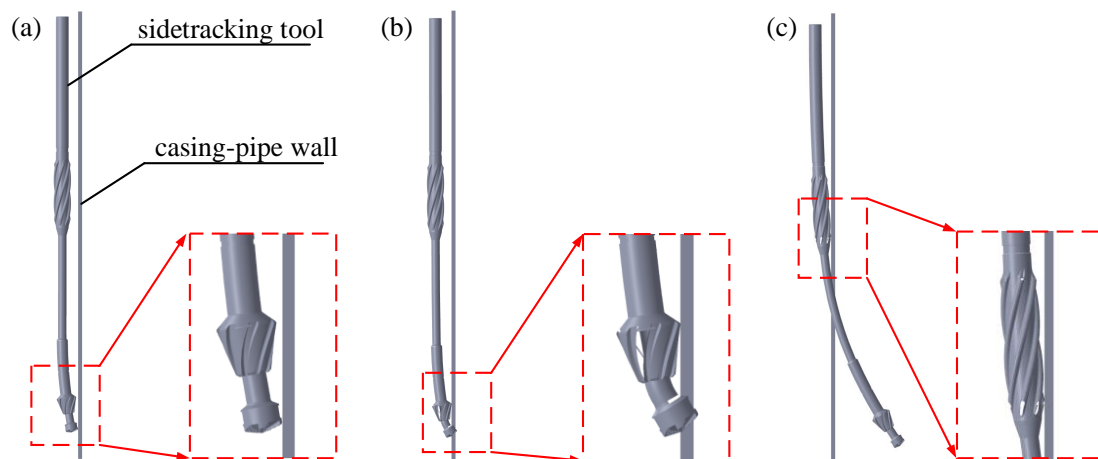


Figure 2. Three typical stages of the sidetracking process: (a) the first stage, (b) the second stage, and (c) the third stage.

The sidetracking process can be divided into three typical stages, as shown in Figure 2. The sidetracking tool is lowered into the casing until the window mill touches the whipstock, which can be considered as the first stage. The second stage occurs when it continues drilling until the pilot mill contacts the whipstock. In the third stage, both the window and pilot mills are included in the formation, and the watermelon mill contacts the whipstock to mill the casing wall for the last time.

2.2. Motion Equation of the Sidetracking Tool

In order to describe the dynamic model, the coordinate system $(x-y-z-\varphi)$ is introduced. Thus, the spatial positions of Parts A, B, and C can be determined by the coordinates $(x_1-y_1-z_1-\varphi_1)$, $(x_2-y_2-z_2-\varphi_2)$, and $(z_3-\varphi_3)$. Parts A, B, and C all rotate around their geometric centers, (x,y) denoting their lateral displacements, and z is their longitudinal displacements. The contact between the sidetracking tool and the casing wall is modeled as linear elasticity. In order to simulate the plane motion of sidetracking tool, linear eccentricity e associated with Part A and Part B is introduced [29]. The mass of Part A is m_1 and the moment of inertia is J_1 . The mass of Part B is m_2 and the moment of inertia is J_2 . The mass of Part C is m_3 and the moment of inertia is J_3 .

2.2.1. The First Stage

During the first stage of the sidetracking process, the windowed shoe section was run, reaching the miter section to begin milling the casing. Then, the kinetic energy of the drill string system can be written as

$$T = \frac{1}{2}m_1(\dot{x}_1^2 + \dot{y}_1^2 + \dot{z}_1^2) + \frac{1}{2}J_1\dot{\varphi}_1^2 + \frac{1}{2}m_2(\dot{x}_2^2 + \dot{y}_2^2 + \dot{z}_2^2) + \frac{1}{2}J_2\dot{\varphi}_2^2 + \frac{1}{2}m_3\dot{z}_3^2 + \frac{1}{2}J_3\dot{\varphi}_3^2 \tag{1}$$

where (·) denotes a time derivative, x_1 and y_1 are the lateral displacements of Part A, and z_1 and φ_1 are the axial and angular displacement, respectively. x_2 and y_2 are the lateral displacement of Part B, and z_2 and φ_2 are the axial and angular displacements, respectively. z_3 and φ_3 are the axial and angular displacements of Part C, respectively.

Euler–Bernoulli beams are used to describe the potential energy V . Let $w(z,t)$ and $\varphi(z,t)$ be the axial and torsional displacements of the sidetracking tool system, respectively, and $u(z,t)$ and $v(z,t)$ be the lateral displacements at $z \in [0, L]$. It is assumed that the deformation is linearly elastic, so V can be constructed as

$$V = \frac{1}{2} \int_0^L \{ EI [(u'')^2 + (v'')^2] + EA(w')^2 + 2GI(\theta')^2 \} dz \tag{2}$$

where, A and I refer to the cross-sectional area and moment of inertia of the string, respectively, and the specific expression is

$$A = \frac{\pi}{4} (D_o^2 - D_i^2) \tag{3}$$

and

$$I = \frac{\pi}{64} (D_o^4 - D_i^4) \tag{4}$$

respectively.

The system is divided into three parts according to the simplified model shown in Figure 3. Therefore, the boundary conditions related to the axial motion of the above system are

$$\begin{cases} w|_{z=0} = v_0t \\ w|_{z=\frac{L}{2}} = z_1 \\ w|_{z=\frac{3L}{4}} = z_2 \\ w|_{z=L} = z_3 \end{cases} \tag{5}$$

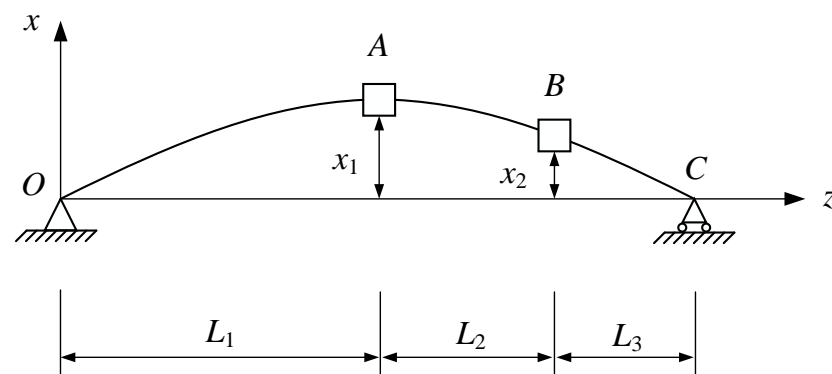


Figure 3. Deformation diagram of the sidetracking tool in the first stage.

Thus, $w(z,t)$ can be represented as

$$w(z, t) = \begin{cases} \frac{z_1 - v_0 t}{L/2} z + v_0 t, & 0 \leq z \leq \frac{L}{2} \\ \frac{z_2 - z_1}{L/4} z - 2z_2 + 3z_1, & \frac{L}{2} < z \leq \frac{3L}{4} \\ \frac{z_3 - z_2}{L/4} z - 3z_3 + 4z_2, & \frac{3L}{4} < z \leq L \end{cases} \quad (6)$$

while the boundary conditions related to the lateral motion are

$$\begin{cases} \theta|_{z=0} = \varphi_t \\ \theta|_{z=\frac{L}{2}} = \varphi_1 \\ \theta|_{z=\frac{3L}{4}} = \varphi_2 \\ \theta|_{z=L} = \varphi_3 \end{cases} \quad (7)$$

Therefore, $\theta(z, t)$ can be represented as

$$\theta(z, t) = \begin{cases} \frac{\varphi_1 - \varphi_t}{L/2} z + \varphi_t, & 0 \leq z \leq \frac{L}{2} \\ \frac{\varphi_2 - \varphi_1}{L/4} z - 2\varphi_2 + 3\varphi_1, & \frac{L}{2} < z \leq \frac{3L}{4} \\ \frac{\varphi_3 - \varphi_2}{L/4} z - 3\varphi_3 + 4\varphi_2, & \frac{3L}{4} < z \leq L \end{cases} \quad (8)$$

In addition, the bending deflection of the sidetracking tool system in the x -direction is shown in Figure 3. The deflection equation and the angle equation of the system in the first stage can be obtained from the shear force and bending moment equations of the system and the boundary conditions of A , B , C and O . Since the bending in the y -direction is symmetric with that in the x -direction, the deformation equations of the window system in the x and y directions can be expressed as

$$u(z, t) = \begin{cases} \frac{2z}{23L^3} [(51x_1 - 24x_2)L^2 - (112x_1 - 96x_2)z^2] & , 0 \leq z \leq \frac{L}{2} \\ -\frac{1}{23L^3} [(144x_1 - 176x_2)L^3] (-928z^3x_1 + 1216z^3x_2 + 1728Lz^2x_1 - 966L^2zx_1 - 2112Lz^2x_2 + 1104L^2zx_2) & , \frac{L}{2} < z \leq \frac{3L}{4} \\ \frac{2L-2z}{23L^3} (225L^2x_1 - 344L^2x_2 + 240z^2x_1 - 416z^2x_2 - 480Lzx_1 + 832Lzx_2) & , \frac{3L}{4} < z \leq L \end{cases} \quad (9)$$

and

$$v(z, t) = \begin{cases} \frac{2z}{23L^3} [(51y_1 - 24y_2)L^2 - (112y_1 - 96y_2)z^2] & , 0 \leq z \leq \frac{L}{2} \\ -\frac{1}{23L^3} [(144y_1 - 176y_2)L^3 - (966y_1 - 1104y_2)L^2z + (1728y_1 - 2112y_2)Lz^2 - (928y_1 - 1216y_2)z^3] & , \frac{L}{2} < z \leq \frac{3L}{4} \\ \frac{2L-2z}{23L^3} [(225y_1 - 344y_2)L^2 - (480y_1 + 832y_2)Lz + (240y_1 - 416y_2)z^2] & , \frac{3L}{4} < z \leq L \end{cases} \quad (10)$$

respectively.

Substituting Equations (6)–(10) into potential energy expression (2), the expression of potential energy can be obtained as

$$V = \frac{EA}{L} \left[2(z_2 - z_1)^2 + 2(z_3 - z_2)^2 + (z_1 - v_0 t)^2 \right] + \frac{GI}{L} \left[2(\varphi_1 - \varphi_t)^2 + 4(\varphi_2 - \varphi_1)^2 + 4(\varphi_3 - \varphi_2)^2 \right] + \frac{EI}{2L^3} \left[\frac{3}{1058} (224x_1 - 192x_2)^2 + \frac{192}{529} (211x_1^2 - 572x_1x_2 + 508x_2^2 + 211y_1^2 - 572y_1y_2 + 508y_2^2) + \frac{3}{1058} (224y_1 - 192y_2)^2 + \frac{192}{529} (225x_1^2 - 780x_1x_2 + 676x_2^2 + 225y_1^2 - 780y_1y_2 + 676y_2^2) \right] \quad (11)$$

In order to describe the viscous damping effect of this sidetracking tool system, Rayleigh dissipation function D is introduced here

$$D = \frac{1}{2} \left[c_a (\dot{z}_1^2 + \dot{z}_2^2 + \dot{z}_3^2) + c_b (\dot{x}_1^2 + \dot{y}_1^2 + \dot{x}_2^2 + \dot{y}_2^2) + c_t (\dot{\varphi}_1^2 + \dot{\varphi}_2^2 + \dot{\varphi}_3^2) \right] \quad (12)$$

$$\{F\} = \left\{ \begin{array}{l} F_{1x} + m_1 e_1 \dot{\varphi}_1^2 \cos \varphi_1 \\ F_{2x} + m_2 e_2 \dot{\varphi}_2^2 \cos \varphi_2 \\ F_{1y} + m_1 e_1 \dot{\varphi}_1^2 \sin \varphi_1 \\ F_{2y} + m_2 e_2 \dot{\varphi}_2^2 \sin \varphi_2 \\ k_w \cdot v_0 t + m_1 g - \text{sign}(\dot{z}_1) \mu_r F_{n1} \\ m_2 g - \text{sign}(\dot{z}_2) \mu_r F_{n2} \\ -W_b - F_b \sin \alpha \\ k_\varphi \cdot \varphi_t - T_1 \\ -T_2 \\ -T_b \end{array} \right\} \tag{18}$$

respectively.

In the above formulas, k_r , k_w , and k_φ are expressed as

$$k_r = \frac{33EI}{L^3}, k_w = \frac{2EA}{L}, k_\varphi = \frac{4GI}{L} \tag{19}$$

respectively.

2.2.2. The Second Stage

In the second stage of the sidetracking process, the window mill has been milled out into the formation, and then, the pilot mill begins milling the casing. The kinetic energy and potential energy of the sidetracking tool system are

$$T = \frac{1}{2} m_1 (\dot{x}_1^2 + \dot{y}_1^2 + \dot{z}_1^2) + \frac{1}{2} J_1 \dot{\varphi}_1^2 + \frac{1}{2} m_2 \dot{z}_2^2 + \frac{1}{2} J_2 \dot{\varphi}_2^2 \tag{20}$$

and

$$V = \frac{1}{2} \int_0^L \{ EI [(u'')^2 + (v'')^2] + EA (w')^2 + 2GI (\theta')^2 \} dz \tag{21}$$

respectively, where, (') denotes a time derivative.

The system is divided into two parts, according to the simplified model shown in Figure 4. Therefore, the boundary conditions related to the axial and lateral motions of the above system are

$$\left\{ \begin{array}{l} w|_{z=0} = v_0 t \\ w|_{z=L/2} = z_1 \\ w|_{z=L} = z_2 \end{array} \right. \tag{22}$$

and

$$\left\{ \begin{array}{l} \theta|_{z=0} = \varphi_t \\ \theta|_{z=L/2} = \varphi_1 \\ \theta|_{z=L} = \varphi_2 \end{array} \right. \tag{23}$$

respectively.

Thus, the $w(z,t)$, $\theta(z,t)$, $u(z,t)$ and $v(z,t)$ are

$$w(z,t) = \left\{ \begin{array}{ll} \frac{z_1 - v_0 t}{L/2} z + v_0 t, & 0 \leq z \leq \frac{L}{2} \\ \frac{z_2 - z_1}{L/2} z - z_2 + 2z_1, & \frac{L}{2} < z \leq L \end{array} \right. \tag{24}$$

$$\theta(z,t) = \left\{ \begin{array}{ll} \frac{\varphi_1 - \varphi_t}{L/2} z + \varphi_t, & 0 \leq z \leq \frac{L}{2} \\ \frac{\varphi_2 - \varphi_1}{L/2} z - \varphi_2 + 2\varphi_1, & \frac{L}{2} < z \leq L \end{array} \right. \tag{25}$$

$$[K] = \begin{bmatrix} k_r & & & & & \\ & k_r & & & & \\ & & 2k_w & -k_w & & \\ & & -k_w & k_w & & \\ & & & & 2k_\varphi & -k_\varphi \\ & & & & -k_\varphi & k_\varphi \end{bmatrix} \tag{33}$$

and

$$\{F\} = \begin{Bmatrix} F_{1x} + m_1 e_1 \dot{\varphi}_1^2 \cos \varphi_1 \\ F_{1y} + m_1 e_1 \dot{\varphi}_1^2 \sin \varphi_1 \\ K_w \cdot v_0 t + m_1 g - \text{sign}(\dot{z}_1) \mu_r F_{n1} \\ -W_b - F_b \sin \alpha \\ K_\varphi \cdot \varphi_t - T_1 \\ -T_b \end{Bmatrix} \tag{34}$$

respectively. In the above formulas, k_r , k_w , and k_φ are expressed as

$$k_r = \frac{48EI}{L^3}, k_w = \frac{2EA}{L} \text{ and } k_\varphi = \frac{2GI}{L} \tag{35}$$

respectively.

2.2.3. The Third Stage

In the third stage, the window mill and pilot mill have finished milling the casing and entered the formation, and the watermelon mill begins milling. At this time, the sidetracking tool system can be regarded as an axial force link element, as shown in Figure 5, and the kinetic energy and potential energy of the system are

$$T = \frac{1}{2} m_1 \dot{z}_1^2 + \frac{1}{2} J_1 \dot{\varphi}_1^2 \tag{36}$$

and

$$V = \frac{1}{2} \int_0^L \{ EI [(u'')^2 + (v'')^2] + EA (w')^2 + 2GI (\theta')^2 \} dz \tag{37}$$

respectively.

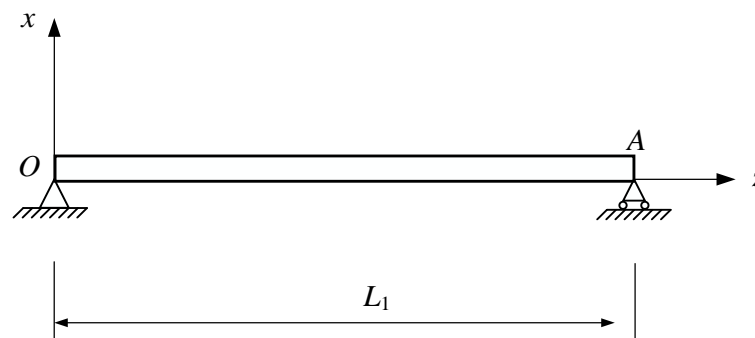


Figure 5. Deformation diagram of the sidetracking tool in the third stage.

Then, the vibration equation of this system is

$$[M]\{\ddot{x}\} + [C]\{\dot{x}\} + [K]\{x\} = \{F\} \tag{38}$$

where, $[M]$, $[C]$, and $[K]$ represent the mass matrix, damping matrix, and stiffness matrix, respectively, and $\{F\}$ is the column vector of the force; their expressions are

$$[M] = \begin{bmatrix} m_1 & \\ & m_1 \end{bmatrix} \quad (39)$$

$$[C] = \begin{bmatrix} c_a & \\ & c_t \end{bmatrix} \quad (40)$$

$$[K] = \begin{bmatrix} k_w & -k_w \\ -k_w & k_w \end{bmatrix} \quad (41)$$

and

$$\{F\} = \begin{Bmatrix} -W_b - F_b \sin \alpha \\ -T_b \end{Bmatrix} \quad (42)$$

respectively.

In the above formulas, k_w is expressed as

$$k_w = \frac{EA}{L} \quad (43)$$

2.3. Contact Model

The sidetracking tool moves within the casing, and its radial displacement should not exceed the clearance between the window mill and the casing inner wall. The radial displacement of the window mill center from the casing center is marked as ρ_i . The radial gap between the window mill and the inner casing is marked as β . The distance of the window mill into the casing wall is marked as δ_i . Here, a judgment parameter λ is introduced to judge whether the mills contact the casing wall. When $\lambda_i = 0$, it indicates that there is no contact between them, while when $\lambda_i = 1$, contact occurs. Their expressions are

$$\rho_i = \sqrt{x_i^2 + y_i^2} \quad (44)$$

$$\beta = \frac{D_c - D_{out}}{2} \quad (45)$$

$$\delta_i = \rho_i - \beta \quad (46)$$

and

$$\lambda_i = \begin{cases} 0, & \delta_i \leq 0 \\ 1, & \delta_i > 0 \end{cases} \quad (47)$$

respectively.

Based on the previous simplifying assumptions, the contact can be described by a linear elastic model. The contact force acting on the sidetracking tool can be divided into two parts, including the normal force F_n and the tangential force F_t due to friction [30], which can be defined as

$$F_{ni} = \lambda_i(k_p\delta_i + c_p v_{ni}) \quad (48)$$

and

$$F_{ti} = \mu_r \left[\tanh(2v_{ri}) + \frac{2v_{ri}}{1 + 4v_{ri}^2} \right] F_{ni} \quad (49)$$

respectively. The normal velocity is

$$v_{ni} = \dot{x}_i \cdot \frac{y_i}{\sqrt{x_i^2 + y_i^2}} + \dot{y}_i \cdot \frac{x_i}{\sqrt{x_i^2 + y_i^2}} \quad (50)$$

If contact occurs, the motion of the sidetracking tool with respect to the casing can be described as pure rolling or sliding. To determine the presence of sliding, the relative velocity between the two faces is marked as

$$v_{ri} = -\dot{x}_i \cdot \frac{x_i}{\sqrt{x_i^2 + y_i^2}} + \dot{y}_i \cdot \frac{y_i}{\sqrt{x_i^2 + y_i^2}} + \frac{D_{out}}{2} \dot{\varphi}_i \quad (51)$$

When $v_r \neq 0$, it means there is only relative sliding, while when $v_r = 0$, it means that there is no relative sliding, but only pure rolling. By superimposing the contact force components along their respective vectors in the x and y directions, the external forces from the casing wall acting on the mill by are calculated as

$$\begin{aligned} F_{xi} &= -F_{ni} \cdot \frac{y_i}{\sqrt{x_i^2 + y_i^2}} + F_{ti} \cdot \frac{x_i}{\sqrt{x_i^2 + y_i^2}} \\ F_{yi} &= -F_{ni} \cdot \frac{x_i}{\sqrt{x_i^2 + y_i^2}} - F_{ti} \cdot \frac{y_i}{\sqrt{x_i^2 + y_i^2}} \end{aligned} \quad (52)$$

The friction moment on the sidetracking tool is

$$T_i = \frac{1}{2} F_{ti} D_{out} \quad (53)$$

The weight on bit and drill bit torque during sidetracking can be defined as

$$W_{ob} = \begin{cases} k_c(z_3 - s_0 \sin(n_b \varphi)), & z_3 < s_0 \sin(n_b \varphi) \\ 0, & z_3 \geq s_0 \sin(n_b \varphi) \end{cases} \quad (54)$$

and

$$T_{ob} = W_{ob} \left[\frac{2}{3} r_{out} f(\dot{\varphi}_3) + \zeta \sqrt{r_{out} \delta_c} \right] \quad (55)$$

respectively, wherein the depth of cut per revolution and the average rate of penetration are

$$\delta_c = \frac{2\pi ROP}{\omega_d} \quad (56)$$

and

$$ROP = c_1 W_0 \sqrt{\omega_d} + c_2 \quad (57)$$

respectively. A continuous function f is used to express the influence of bit speed on bit torque [31], and its expression is

$$f(\dot{\varphi}_3) = \frac{2}{\pi} a \tan(\varepsilon \dot{\varphi}_3) \left(\frac{\mu_e - \mu_d}{1 + \tau |\dot{\varphi}_3|} + \mu_d \right) \quad (58)$$

3. Simulation of the Sidetracking Tool Motion Process

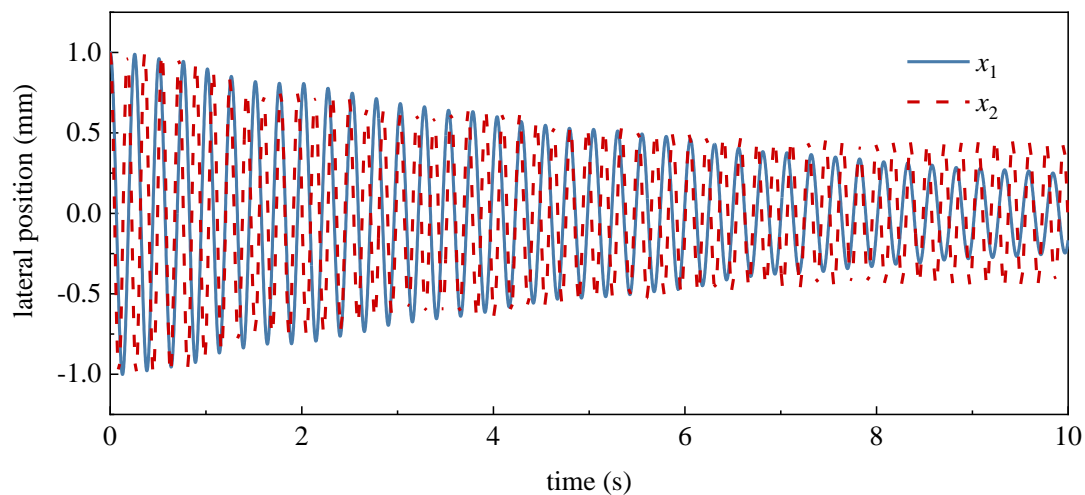
A numerical procedure is used to solve the obtained equations system, which can be solved using the Runge–Kutta method. Some system parameters involved in the calculations and their specific values are listed in Table 1, which represent typical situations in sidetracking operations.

3.1. The First Stage

Analyzing the curve diagram of displacement with respect to time variation can better describe the movement of the sidetracking tool. Figures 6 and 7 both show the historical curve of time displacement within the test time. Figure 6 shows the change diagram of lateral displacement with respect to time of Parts A and B, and Figure 7 shows the time variation of the angular displacements of Parts A, B, and C. In the above two figures, x_1 and x_2 represent the lateral displacement of Parts A and B, respectively, and φ_1 , φ_2 , and φ_3 represent the angular displacement of Parts A, B, and C, respectively. Figure 6 only discusses the lateral displacement in the x -direction because the bending in the y -direction is symmetrical with the bending in the x -direction.

Table 1. System parameters values used for numerical study.

Quantities	Variable	Value	Units
Unbalanced mass on BHA	m_b	10	kg
Tool external diameter	D_{out}	215.9	mm
Tool internal diameter	D_{in}	86.1	mm
Casing internal diameter	D_c	244.5	mm
Linear eccentricity	e	8	mm
Elastic modulus	E	2.1×10^{11}	Pa
Shear modulus	G	7.7×10^{10}	Pa
Density	ρ	7800	kg/m ³
Distance between restraint end and watermelon mill	L_1	640	mm
Distance between pilot mill and watermelon mill	L_2	320	mm
Distance between the window mill and the pilot mill	L_3	320	mm
Whipstock angle	α	2	°
Static friction coefficient	μ_e	0.35	
Dynamic friction coefficient	μ_d	0.1	
Initial weight on bit	W_0	30×10^3	N
Supporting force of whipstock	F_{ob}	200×10^3	N
Initial speed	θ_1	3.14	rad/s
Initial angle	φ_t	10	°
Contact stiffness of tool and casing	k_p	1×10^8	N/m
Contact stiffness of window mill	k_c	25×10^3	
Damping of tool and casing	c_p	5×10^3	N·s/m
Steepness parameter	χ	0.5	
Empirical constants	c_1	1.35×10^{-8}	
Empirical constants	c_2	1.9×10^{-4}	
Forced parameters related to borehole irregularity	s_0	0.001	
Dimensionless coefficient	ζ	0.1	
Bit coefficient	n_b	3	

**Figure 6.** Schematic diagram of lateral displacements x_1 and x_2 with respect to t .

The length of the sidetracking tool analyzed in this paper is 1280 mm, and within this measurement range, only a small range of vibration occurs. In Figure 6, the amplitude of the window mill and the pilot mill at the initial time in the x direction is relatively large, and the amplitude gradually decreases with the passage of time. This phenomenon indicates that the window mill rolls continuously in the axial direction. The amplitude of φ_3 is always larger than φ_1 and φ_2 in the measured range. In the first stage of sidetracking, the window mill just begins to contact the whipstock, and in addition to the friction of casing wall, the system is also subjected to the lateral support of the whipstock, while the

movements of the other two parts are still in the casing, so the dynamic response of Part C is more obvious and larger than that of the other two parts.

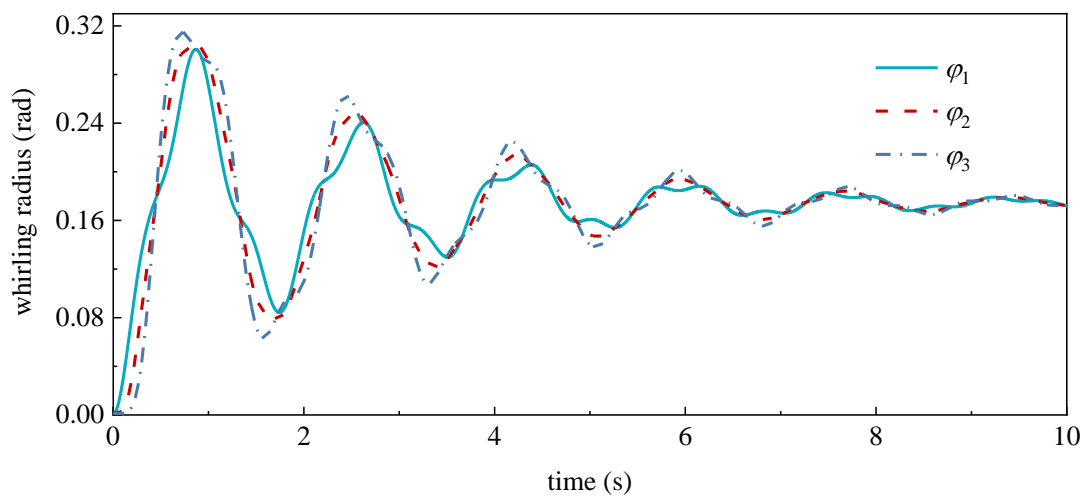


Figure 7. Schematic diagram of angular displacements φ_1 , φ_2 and φ_3 with respect to t .

Figure 8 shows the angular velocity variation of the three Parts A, B, and C with respect to time in the first stage. The rotation direction varies continuously between forward and backward during the time period covered by the simulation, and all three curves are faster in the first half of the period. This model predicts the contact between the sidetracking tool and the casing, but the sidetracking tool is short, and its vibration amplitude is smaller than the gap between the shoe and the casing wall. The vibration is finally stabilized as a limit ring behavior due to the presence of dissipative effects such as friction.

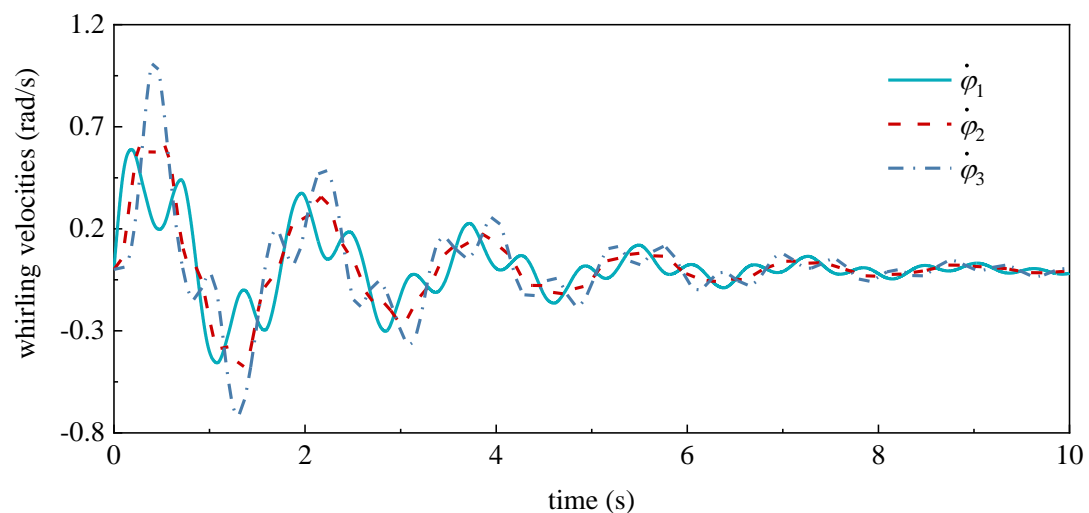


Figure 8. Schematic diagram of angular velocity of Parts A, B and C with respect to t , respectively.

Figure 9 shows the lateral motion trajectory of Part C. It can be seen from the figure that the window mill can only roll back and forth in the direction parallel to the surface of the whipstock. It is worth noting that the vibration trajectory shape changes from the vortex shape to the X reciprocating shape, which is very different from the behavior of conventional drilling tools. Its vibration amplitude is smaller than the gap between the window mill and the casing wall, and there is no random collision with the casing wall. The maximum lateral displacement is 3.30 mm.

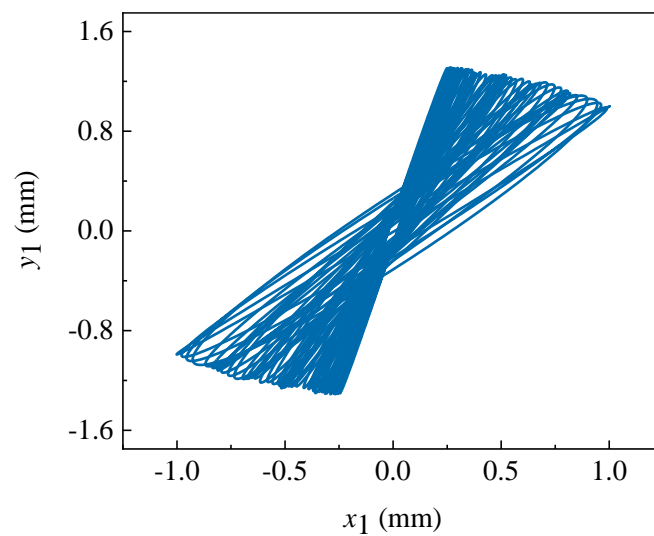


Figure 9. The movement trajectory of the window mill.

3.2. The Second Stage

During the second stage of the sidetrack process, the window mill is milled into the formation, and the pilot mill begins to mill the casing. The research objects in this stage are Parts A and B.

Figures 10 and 11 both show the historical curve of time-displacement in the test time. Figure 10 shows the lateral displacement change diagram of Part A with respect to time, and Figure 11 shows the angular displacement change diagram of Parts A and B with respect to time. In the above two figures, x_1 and y_1 represent the lateral displacement of Part A, respectively, and φ_1 and φ_2 represent the angular displacement of Parts A and B, respectively.

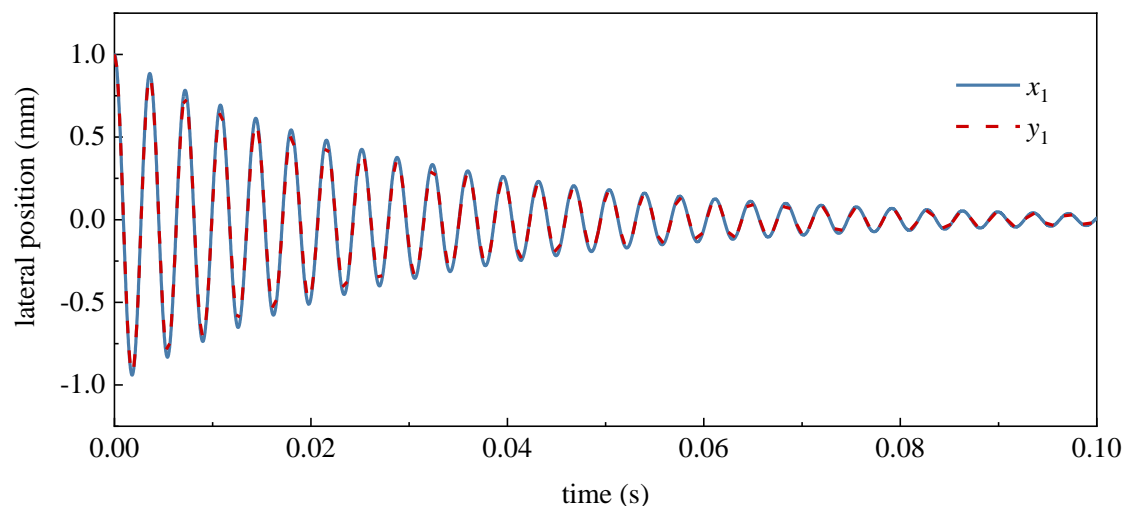


Figure 10. Schematic diagram of lateral displacements x_1 and y_1 with respect to t .

From Figure 10, it can be seen that the amplitude of the pilot mill is larger in the lateral direction at the initial moment, and it gradually decreases with time. This phenomenon indicates that the pilot mill continuously tumbles in the axial direction. The angular displacement curve (Figure 11) shows obvious vibration in the first half of the study period, and gradually levels off in the second half. In addition, φ_2 is always larger than φ_1 . Figure 12 shows the angular speed variation of the two Parts A, B with respect to time in the second stage. The angular speed curve shown in Figure 12 has obvious vibration in the

first half of the study period, and gradually level off in the second half. In addition, the angular speed of Part B is always larger than the angular speed of Part A.

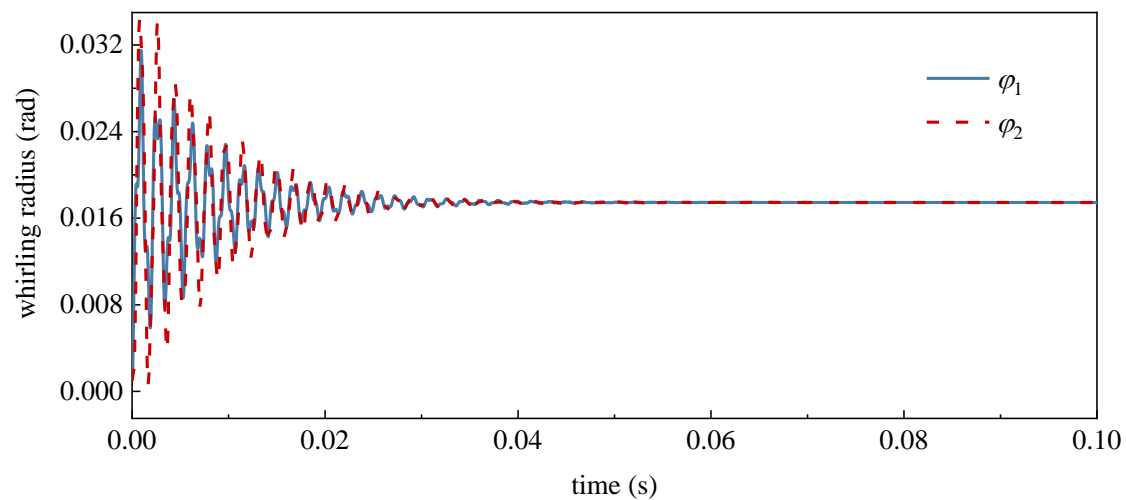


Figure 11. Schematic diagram of angular displacements φ_1 and φ_2 with respect to t .

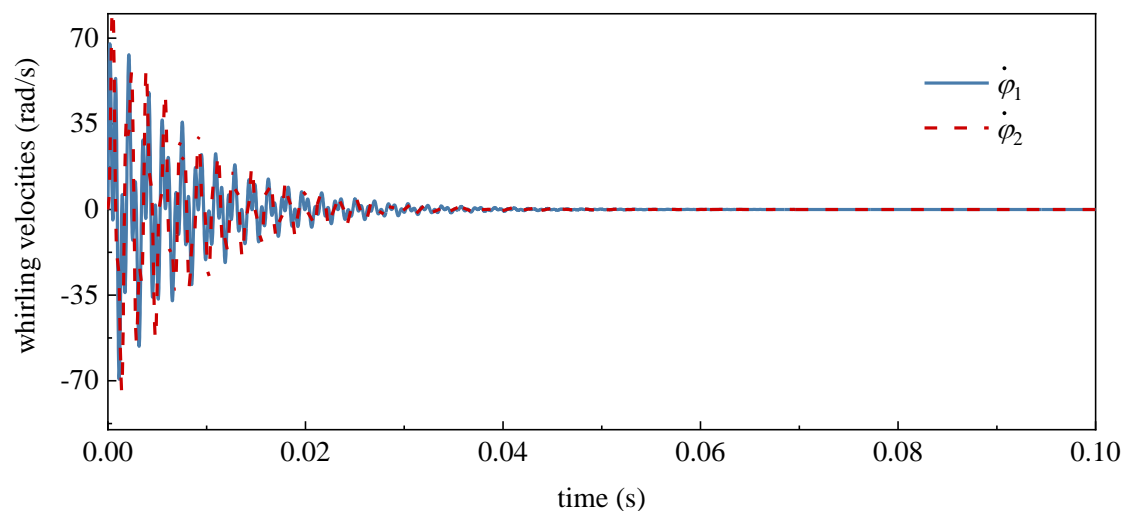


Figure 12. Schematic diagram of angular velocity with respect to t .

In the second stage of the open window, the window mill has entered the formation, and the pilot mill is in contact with the whipstock; thus, it is subject to the frictional force of the casing wall and the lateral support force of the whipstock. Therefore, the dynamic response of Part B is more obvious compared with the other two parts, and the amplitude is larger. Over time, the motion of the sidetracking tools all gradually stabilized.

The lateral movement trajectory of Part B is shown in Figure 13. It can be seen that the pilot mill rolls back and forth in the direction parallel to the surface of the whipstock. The pilot mill is located in the middle of the window mill and the watermelon mill in the axial direction. Both of its ends are subjected to tension and restriction, so its motion range is smaller than that of the window mill, which is in the first stage. The maximum lateral displacement at this moment is 2.74 mm.

3.3. The Third Stage

In the third stage, the window and pilot mills have entered the formation, and the watermelon mill is in the window position. In this case, the sidetracking tool system can be considered as a cantilever beam structure, with a fully restrained upper end and a lower end subject to the lateral forces provided by the whipstock and the weight on bit

generated during the drilling process. Numerical simulation is used to calculate the lateral displacement of the tool system under the action of weight on bit and lateral force. The specific steps are as follows.

1. The upper end of the tool system is fully constrained, and the lateral force in the positive Z-axis is applied to the ground sole circle at the lower end. The lateral force is 23.3 kN.
2. Subsequently, the upper end of the sidetracking tool is fully constrained, which has been deformed at this moment, and a WOB of 5 t and a torque of 130 kN·m are applied to its lower surface.
3. The lateral displacements of the sidetracking tool under the weight on bit, torque, and lateral force are shown in Figure 14.

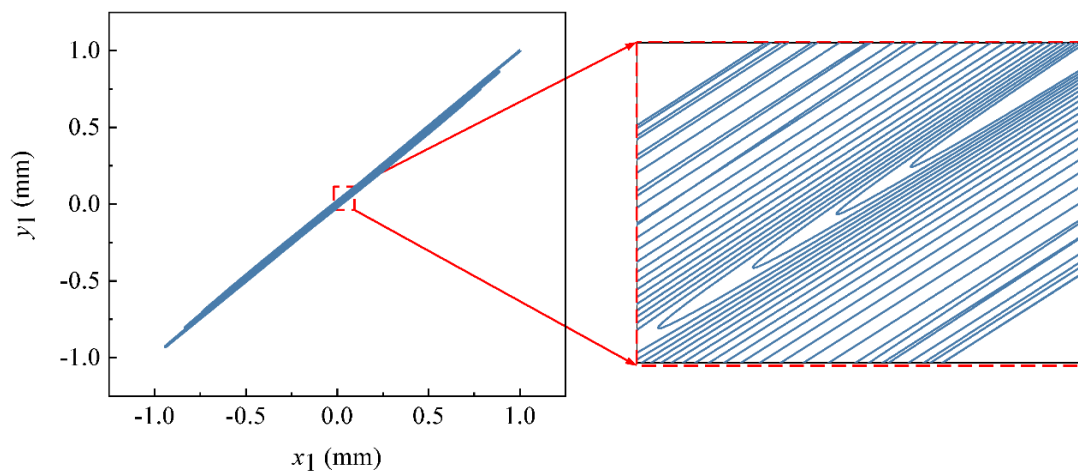


Figure 13. The movement trajectory of the pilot mill.

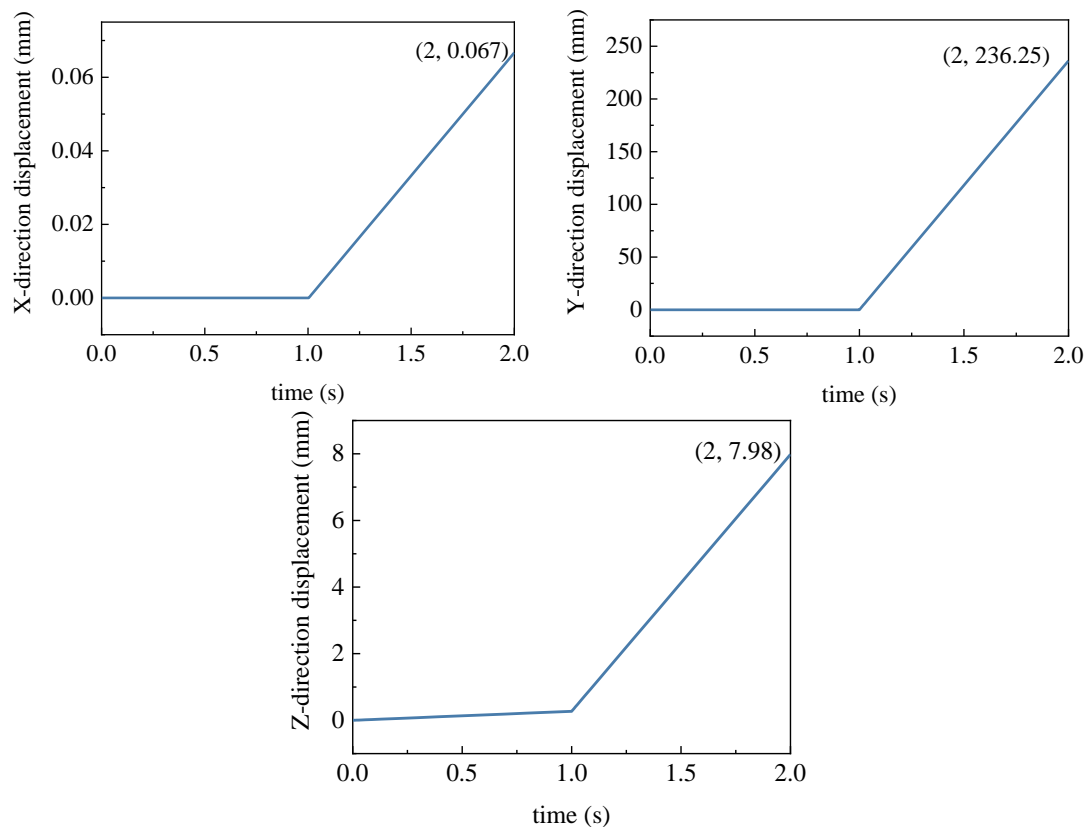


Figure 14. Displacement of BHA.

In Figure 14, the first half of the curve indicates that the tool has not yet touched the whipstock and is only subject to weight on bit and torque, producing only a small lateral displacement, which is negligible. While the latter half indicates that the tool has contacted the whipstock. The lateral force of the whipstock acts on the tool y -direction, so the displacement in this direction is the largest. None of the external forces on the tool had a large effect on the displacement in the x -direction. From the results of the numerical simulation, it can be seen that the maximum lateral displacement in the x -direction of the sidetracking tool is 0.067 mm.

3.4. Case Analysis

Through the above analysis, the window width, which is derived from the action of an arbitrary size casing and the mills, can be calculated. A longitudinal profile of the casing is taken from the centerline of the casing. In this case, the plane is perpendicular to the casing wall, and the Cartesian coordinate system is established, as shown in Figure 15.

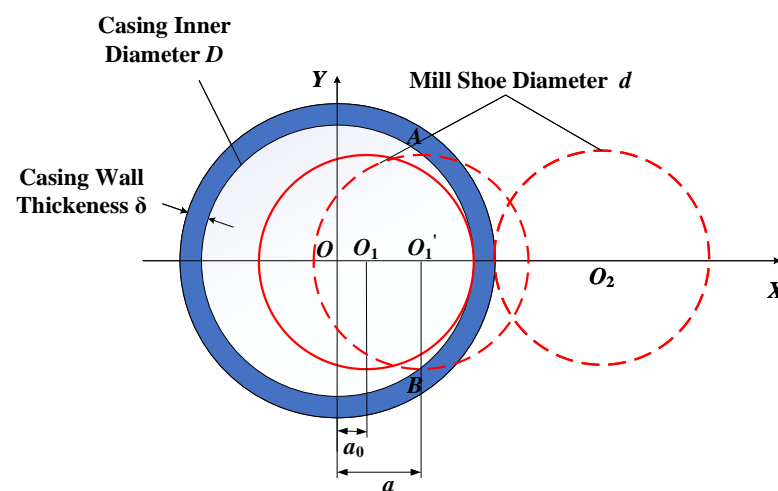


Figure 15. Schematic to model the lateral motions of window mill.

The central point of casing on this plane coincides with the central point of the window mill, and this point is set as the origin of the coordinates O . The forward direction of the window mill is taken as the X axis, and the direction perpendicular to the X axis is taken as the Y axis. The casing inner diameter, marked as D , represents the thickness, marked as δ , and the outer diameter is marked as $D + \delta$. The outer diameter of the window mill is marked as d . γ represents the bevel angle of the whipstock, and a represents the distance between the center of the casing and the center of the window mill. The window width produced by the window mill on the casing can be regarded as the length between the intersection points of two circles on the XY plane, as shown in Figure 15. The derived theoretical formula for the window width is

$$W = 2\sqrt{\frac{D^2 + d^2}{8} - \frac{(\frac{D-d}{2} + x)^2}{4} - \frac{(D^2 - d^2)^2}{64(\frac{D-d}{2} + x)^2}}, x \in [0, d + \delta] \quad (59)$$

where x is the distance between the tool cross section center and the casing cross section center. When $D = 244.48$ mm, $d = 184.15$ mm, and $\delta = 13.84$ mm, the ideal window width calculated by Equation (59) is $W = 368.23$ mm.

The schematic diagram of the window result formed by the sidetracking tool milling casing wall under stress is shown in Figure 16, where curve (1) represents the theoretical window profile calculated by Equation (59). Curve (2) represents the window profile formed by the window mill, and the maximum lateral displacement generated is 3.30 mm. Curve (3) is the window profile formed by the pilot mill, and the maximum lateral displacement generated by it is 2.74 mm. Curve (4) is the profile formed by watermelon mill,

whose maximum lateral displacement is 0.07 mm. Therefore, the maximum width of the final window is 374.34 mm.

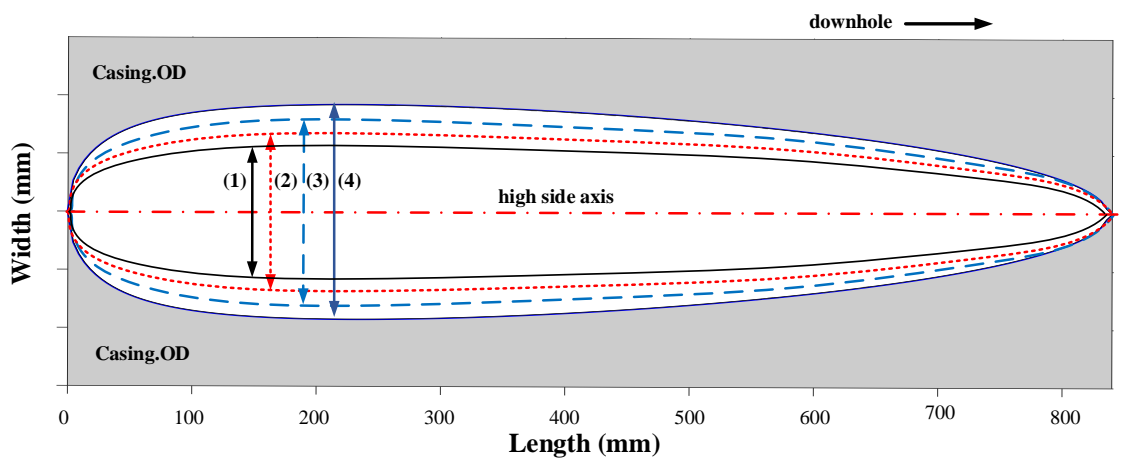


Figure 16. Schematic diagram of the window profile.

4. Conclusions

A study of the coupled axial, lateral, and torsional vibrations of an actively controlled sidetracking tool has been presented and some dynamic models have been proposed, including a ten degrees of freedom, six degrees of freedom, and a two degree of freedom dynamics model, which can be used to analyze the effect of the sidetracking tool system vibration on the casing window profile.

1. The sidetracking tool is taken as the research focus during window opening, and the simplified physical model is established including Parts A, B, and C. The vibration model of the sidetracking tool is obtained according to the Lagrange equation, which can be solved by the Runge–Kutta numerical method. This model can be used to analyze the force and motion process of different mills during the sidetracking.
2. The dynamic model is numerically solved by Runge–Kutta method, and the dynamic responses of different parts of the sidetracking tool at different stages are obtained. The analysis shows that regarding the drilling of the sidetracking tool, the vibration amplitude of the mills colliding with the whipstock is the largest. Its displacement and angular velocity are larger than those of the other parts. The vibration trajectory pattern of the sidetracking tool is different from that of the conventional drilling tool due to the influence of the whipstock, which changes from the general whirling motion pattern to the X reciprocating pattern, and the vibration amplitude decreases.
3. The sidetracking tool analyzed in this paper does not include the drill pipe, but only the mills. Within this measurement range, a small range of vibration occurs, which is smaller than the gap between the mill and the casing wall.
4. The window profile is widened by the sidetracking tool vibration deformation, and the extension of the window width by the window mill and the pilot mill are 3.30 mm and 2.74 mm, respectively. The extension of the window width by the watermelon mill is 0.07 mm, so the maximum window width formed by the sidetracking tool is 374.34 mm.

During the casing sidetracking process, the actual window shape will also be affected by parameters such as mill shape, casing material, and formation hardness. In the next study, more influencing factors will be considered to further improve the accuracy and applicability of window opening tools.

Author Contributions: Conceptualization, X.Z. and B.Z.; methodology, X.Z.; software, W.Z.; formal analysis, W.Z.; investigation, W.Z., Y.L. and P.J.; data curation, Y.L. and P.J.; writing—original draft preparation, X.Z., W.Z., Y.L. and P.J.; writing—review and editing, S.X., B.Z. and Y.X.; visualization, X.Z. and W.Z.; supervision, S.X. and B.Z.; funding acquisition, S.X. All authors have read and agreed to the published version of the manuscript.

Funding: This research was funded by [the National Key Research and Development Program of China] grant number [No. 2019YFC1509204] and [the Independent Innovation Research Program of China University of Petroleum (East China)] grant number [No.27RA2215005].

Conflicts of Interest: The authors declare no conflict of interest.

References

- Kong, C.; Zhang, D.; Liang, Z.; Cai, R. Mechanical analysis of drill bit during dual-casing sidetracking. *J. Pet. Sci. Eng.* **2017**, *159*, 970–976. [CrossRef]
- Yang, Y.; Yang, Y.; Ren, H.; Qi, Q.; Chen, X. Research on the working mechanism of the PDC drill bit in compound drilling. *J. Pet. Sci. Eng.* **2020**, *185*, 106647. [CrossRef]
- Yuan, Y.; Qi, Z.; Yan, W.; Zhang, J.; Chen, C. Old well sidetracking selection standards: Sulige low-permeability gas field, China. *J. Pet. Explor. Prod. Technol.* **2020**, *10*, 1699–1709. [CrossRef]
- Han, Y.; Ai, Z.; Kuang, Y.; Liu, J.; Yang, W. Nonlinear dynamic modeling of drill string in horizontal well—A geometrically exact approach. *J. Pet. Sci. Eng.* **2018**, *172*, 1133–1152. [CrossRef]
- Feng, T.; Bakshi, S.; Gu, Q.; Yan, Z.; Chen, D. Design optimization of bottom-hole assembly to reduce drilling vibration. *J. Pet. Sci. Eng.* **2019**, *179*, 921–929. [CrossRef]
- Divenyi, S.; Savi, M.A.; Franca, L.F.P.; Weber, H.I. Nonlinear dynamics and chaos in systems with discontinuous support. *Shock Vib.* **2006**, *13*, 315–326. [CrossRef]
- Richard, T.; Gernay, C.; Detournay, E. A simplified model to explore the root cause of stick–slip vibrations in drilling systems with drag bits. *J. Sound Vib.* **2007**, *305*, 432–456. [CrossRef]
- Yigit, A.; Christoforou, A. Coupled torsional and bending vibrations of actively controlled drillstrings. *J. Sound Vib.* **2000**, *234*, 67–83. [CrossRef]
- Gernay, C.; Denoël, V.; Detournay, E. Multiple mode analysis of the self-excited vibrations of rotary drilling systems. *J. Sound Vib.* **2009**, *325*, 362–381. [CrossRef]
- Choi, S.H.; Pierre, C.; Ulsoy, A.G. Consistent modeling of rotating timoshenko shafts subject to axial loads. *J. Vib. Acoust.* **1992**, *114*, 249–259. [CrossRef]
- Ahmadian, H.; Nazari, S.; Jalali, H. Drill string vibration modeling including coupling effects. *Int. J. Ind. Eng. Prod. Res.* **2007**, *18*, 59–66. Available online: <http://ijiepr.iust.ac.ir/article-1-30-fa.html> (accessed on 1 October 2022).
- Nandakumar, K.; Wiercigroch, M. Stability analysis of a state dependent delayed, coupled two DOF model of drill-stringvibration. *J. Sound Vib.* **2013**, *332*, 2575–2592. [CrossRef]
- De Moraes, L.P.; Savi, M.A. Drill-string vibration analysis considering an axial-torsional-lateral nonsmooth model. *J. Sound Vib.* **2018**, *438*, 220–237. [CrossRef]
- Xie, D.; Huang, Z.; Ma, Y.; Vaziri, V.; Kapitaniak, M.; Wiercigroch, M. Nonlinear dynamics of lump mass model of drill-string in horizontal well. *Int. J. Mech. Sci.* **2020**, *174*, 105450. [CrossRef]
- Mohammadzadeh, M.; Shahgholi, M.; Arbabtafti, M.; Yang, J. Vibration analysis of the fully coupled nonlinear finite element model of composite drill strings. *Arch. Appl. Mech.* **2020**, *90*, 1373–1398. [CrossRef]
- Mohammadzadeh, M.; Arbabtafti, M.; Shahgholi, M.; Yang, J. Nonlinear vibrations of composite drill strings considering drill string-wellbore contact and bit-rock interaction. *Arch. Appl. Mech.* **2022**, *92*, 2569–2592. [CrossRef]
- Wang, P.; Ni, H.; Wang, X.; Wang, R. Modelling the load transfer and tool surface for friction reduction drilling by vibrating drill-string. *J. Pet. Sci. Eng.* **2018**, *164*, 333–343. [CrossRef]
- Tian, J.; Li, G.; Dai, L.; Yang, L.; He, H.; Hu, S. Torsional vibrations and nonlinear dynamic characteristics of drill strings and stick-slip reduction mechanism. *J. Comput. Nonlinear Dyn.* **2019**, *14*, 4043564. [CrossRef]
- Tian, J.; Liu, Y.; Xiong, J.; Wen, F.; Liu, G. Analysis of drill string's vibration characteristics based on sliding mode-PI controller. *J. Vib. Eng. Technol.* **2022**, *10*, 919–927. [CrossRef]
- Ritto, T.G.; Ghandchi-Tehrani, M. Active control of stick-slip torsional vibrations in drill-strings. *J. Vib. Control* **2018**, *25*, 194–202. [CrossRef]
- Xu, Y.; Zhang, H.; Guan, Z. Dynamic characteristics of downhole bit load and analysis of conversion efficiency of drill string vibration energy. *Energies* **2021**, *14*, 229. [CrossRef]
- Sassi, S.; Renno, J.; Zhou, H.; Baz, A. Experimental investigation of the vibration control of nonrotating periodic drill strings. *J. Vib. Acoust.* **2021**, *143*, 4049942. [CrossRef]
- Sadeghi, A.N.; Arıkan, K.B.; Özbek, M.E. Modelling and controlling of drill string stick slip vibrations in an oil well drilling rig. *J. Pet. Sci. Eng.* **2022**, *216*, 110759. [CrossRef]

24. Sarker, M.; Rideout, D.G.; Butt, S.D. Dynamic model for 3D motions of a horizontal oilwell BHA with wellbore stick-slip whirl interaction. *J. Pet. Sci. Eng.* **2017**, *157*, 482–506. [[CrossRef](#)]
25. Liu, Y.; Gao, D. A nonlinear dynamic model for characterizing downhole motions of drill-string in a deviated well. *J. Nat. Gas Sci. Eng.* **2017**, *38*, 466–474. [[CrossRef](#)]
26. Wang, J.; Xue, Q.; Li, L.; Huang, L.; Li, F.; Liu, B. Influence of flex-sub on mechanical properties of rotary steerable drilling system. *Mech. Sci.* **2020**, *11*, 285–297. [[CrossRef](#)]
27. Navarro-López, E.M. An alternative characterization of bit-sticking phenomena in a multi-degree-of-freedom controlled drillstring. *Nonlinear Anal. Real World Appl.* **2009**, *10*, 3162–3174. [[CrossRef](#)]
28. Tian, J.; Yang, Y.; Yang, L. Vibration characteristics analysis and experimental study of horizontal drill string with wellbore random friction force. *Arch. Appl. Mech.* **2017**, *87*, 1439–1451. [[CrossRef](#)]
29. Liao, C.-M.; Vlajic, N.; Karki, H.; Balachandran, B. Parametric studies on drill-string motions. *Int. J. Mech. Sci.* **2012**, *54*, 260–268. [[CrossRef](#)]
30. Caijin, Y.; Zaibin, C.; Wei, J.; Shiquan, J.; Gexue, R. A Multibody dynamic model of drillstring for torque and drag analysis. *J. Offshore Mech. Arct. Eng.* **2015**, *137*, 31403. [[CrossRef](#)]
31. Christoforou, A.; Yigit, A. Fully coupled vibrations of actively controlled drillstrings. *J. Sound Vib.* **2003**, *267*, 1029–1045. [[CrossRef](#)]

Disclaimer/Publisher’s Note: The statements, opinions and data contained in all publications are solely those of the individual author(s) and contributor(s) and not of MDPI and/or the editor(s). MDPI and/or the editor(s) disclaim responsibility for any injury to people or property resulting from any ideas, methods, instructions or products referred to in the content.